Revista Virtual de Química

Article

http://dx.doi.org/10.21577/1984-6835.20240038

Synthesis, Characterization and Application of Magnetic Nanoparticles for the Photodegradation of Tartrazine Yellow Dye

Síntese, Caracterização e Aplicação de Nanopartículas Magnéticas para Fotodegradação do Corante Amarelo Tartrazina

Marccus V. A. Martins,[a,] Thayná M. G. Santos,[b] Elaine A. F. Braga,[c] Nathália S. Tateno,[d] Jocélia P. C. Oliveira[d]*

[a]Instituto Federal Goiano, Campus Avançado Catalão, Gerência de Ensino, CEP 75701-655, Catalão-GO, Brasil
[b]Instituto Federal de Goiás, Campus Aparecida de Goiânia, Departamento de Áreas Acadêmicas, CEP 74968-755, Aparecida de Goiânia-GO, Brasil
[c]Instituto Federal de Goiás, Campus Inhumas, Departamento de Áreas Acadêmicas, CEP 74968-755, Inhumas-GO, Brasil
[d]Universidade Federal de Catalão, Instituto de Química, CEP 75705-220, Catalão-GO, Brasil

***E-mail:** marccus.victor@ifgoiano.edu.br

Recebido: 12 de Abril de 2024

Aceito: 11 de Julho de 2024

Publicado online: 15 de Julho de 2024

Iron oxide magnetic nanoparticles (MNps) stabilized in the poly(diallyldimethylammonium) chloride (PDAC) polymer were employed to increase the photodegradation of tartrazine yellow dye. MNps stabilized in the PDAC matrix formed the MNp-PDAC nanohybrid, with a medium diameter of 22 nm. A solution efficiency of 30% was obtained in the dye degradation without the nanohybrid, which increased to 96% with MNps, after 120 minutes. This greater dye removal efficiency in the presence of MNps was attributed to adsorption due to electrostatic interaction of the PDAC's positive site and the negative charge of tartrazine yellow dye, which brings the azo group of the dye closer to the surface of the nanohybrid. The kinetic parameters obtained from the Langmuir-Hinshelwood linearization for this photodegradation system confirmed the efficiency of the photocatalyst in removing the dye from the solution used in this work.

Keywords: Nanohybrid; photodegradation; MNp; dye.

1. Introduction

The development of new technologies for the removal of dyes in wastewater has attracted attention to new nanomaterials and new strategies to increase the efficiency of photodegradation.[1] Various dyes have a complex chemical structure which hardly undergoes natural degradation, hence contaminating the environment.[2-6] Rapid and efficient removal of these dyes has aroused interest in the development of various technologies. Among them, the degradation of dyes by light in the ultraviolet (UV) region is known for being fast. In aqueous media and in the presence of oxygen, dye photodegradation occurs by generating radicals (*e.g.* ,) with a high oxidative power, which attack specific groups in the dye chemical structure.[6-9] These radicals may be generated by photoinduction of an electron in the valence band () and a positive hole in the conduction band () in a photocatalyst.[8,10,11]

As strategic materials, the literature has reported several semiconductors as photocatalysts, such as TiO_2,[7,9] ZnO,[12,13] $MgFe_2O_4$–$MgTiO_3$,[14] Bi_2WO_6/BiOI@Fe_3O_4[15] and γ-Fe_2O_3/Fe_3O_4/SiO_2,[16] to increase the production of / pairs and increase dye removal efficiency. Moreover, nanoscale photocatalysts offer high surface area and high surface reactivity, which increases the efficiency of photodegradation.[17-19] In this aspect, the use of magnetic nanoparticles (MNps) combines the advantages of nanoscale properties with the possibility of easily removing magnetic photocatalysts from the aqueous medium by applying an external magnetic field.[20,21] Several works use magnetic nanomaterials as photocatalysts in the degradation of dyes, as reported by Dlugosz and co-authors,[22] Fardood and co-authors,[23] Lónski and co-authors[24] and Jadhav and co-authors,[25] among others. However, the production of these nanomaterials is usually carried out in two or more synthesis steps to better control the morphological and optical properties, while this work proposes the synthesis of magnetite nanoparticles (Fe_3O_4 Nps) based on the coprecipitation method in a single step, as a quick and easy synthesis route strategy for application in the photodegradation of tartrazine yellow dye.

The synthesis of nanoparticles in aqueous medium requires the use of a stabilizing matrix, which inhibits agglomeration between particles.[26,27] In view of this problem, several studies have reported the use of organic polymers as a stabilizing matrix to inhibit the formation of agglomerates.[27] Depending on the application, the stabilizing polymer may also perform other functions, *e.g.*, associative recognition with other structures.

In this work, we strategically used the poly(diallyldimethylammonium) chloride (PDAC) polymer to perform two functions: first, to inhibit the excessive growth of iron oxide magnetic nanoparticles, and second, to promote interaction of the tartrazine yellow dye with the surface of nanoparticles. This interaction between the polymer and the dye was strategically employed to increase the removal efficiency.

2. Experimental

2.1. Synthesis of magnetic nanoparticles (MNp)

All the reagents used for the synthesis of Fe_3O_4 were analytical grade and used without further purification. Ferric chloride $FeCl_3$, ferrous chloride $FeCl_2$, ammonium hydroxide NH_4OH, and poly(diallyldimethylammonium chloride) (PDAC) were purchased from Aldrich.

MNps were synthesized by the coprecipitation method with some modifications.[28] First, all solutions were prepared using distilled water: 25 mL of $FeCl_2$ (1 mmol L^{-1}), 50 mL of $FeCl_3$ (1 mmol L^{-1}) and 50 mL of PDAC polymer (0.5 mmol L^{-1}) were vigorously stirred at 60 °C. Then, 300 mL of ammonium hydroxide (NH_4OH) (7 mol L^{-1}) were added to the mixture containing the salts and the polymer. The system was kept under stirring at 60 °C for 1 hour until the solution changed from yellow to brown.

2.2. Photodegradation of tartrazine yellow dye

Water soluble dye, tartrazine (Figure 1), selected for the present investigation. For photocatalytic degradation, 50 ppm stock solution of tartrazine dye was prepared in double distilled water.

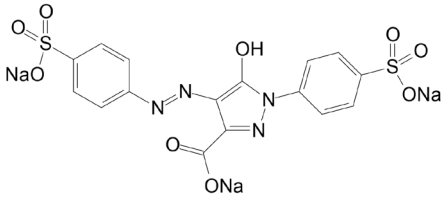

Figure 1. Chemical structure of the tartrazine yellow dye

Photodegradation experiments were carried out with a solution of 50 ppm of tartrazine yellow dye. First, 0.5 g L^{-1} of MNps were added directly to 100 mL of tartrazine yellow dye solution and placed in a Labmade photo-reactor. Then, the mixture was placed under magnetic stirring and subjected to the UV irradiation of a mercury vapor lamp of 125 W. The mixture was stirred for 1 hour in the absence of light to promote the adsorption of tartrazine on the photocatalyst (which was considered as time 0 in all graphs). After 1 hour, the reactor lamp was turned on and the reaction was conducted for 120 min and at 15 min intervals, 3 mL of the solution was collected to be analyzed by the UV–Vis spectrophotometer at a maximum wavelength of 420 nm, which reflects the maximum absorbance of the azo group of tartrazine. For each aliquot removed, an external magnetic field was applied in order to separate the nanocatalyst from the solution.

2.3. Kinetic parameters

To analyze the kinetic parameters, the Langmuir-Hinshelwood model was used, according to Equation 1.

$$\frac{C_e}{q_e} = \frac{1}{q_m \times K_L} + \frac{1}{q_m} \times C_e \quad (1)$$

where $\mathbf{C_e}$ is tartrazine concentration in the equilibrium state (mg L^{-1}), $\mathbf{q_e}$ is the amount of dye that was adsorbed to equilibrium (mg g^{-1}), $\mathbf{K_L}$ is the equilibrium constant, and $\mathbf{q_m}$ is the maximum amount that can be adsorbed in the adsorption process. Langmuir constants ($\mathbf{K_L}$ and $\mathbf{q_m}$) were determined by linear regression of the linearized equation. This model assumes that, at equilibrium, the number of sites adsorbed on the surface of MNps is constant, and only one substrate is adsorbed on each site.

2.4. Microscopic and spectroscopic characterization

Ultraviolet-visible spectroscopy (UV–VIS) experiments were performed utilizing the spectrophotometer Varian at 25 °C, in the range of 200 to 800 nm, using a long quartz cuvette (1 cm). The morphology and size of MNps were analyzed in a field emission gun scanning electron microscope (FEG-SEM) Jeol Brand, JSM-7100FT, using the secondary electrons. For the FEG-SEM analysis, a small amount of MNps was dripped on carbon tape.

3. Results and Discussion

3.1. Synthesis of magnetic nanoparticles (MNp)

MNps were obtained by the coprecipitation[24] of and ions in the presence of the PDAC polymer. After the addition of 300 mL of ammonium hydroxide (7 mol L^{-1}) in the PDAC-MNp nanohybrid, the solution changed its color from yellow to brown, as illustrated in Figures 2a and 2b.

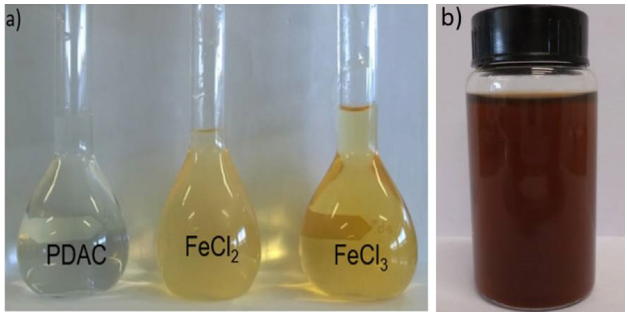

Figure 2. (a) Solutions of PDAC, $FeCl_2$ and $FeCl_3$ (b) suspension of the PDAC-MNp nanohybrid

Figure 3a shows the UV-VIS spectral of the solution containing $FeCl_2$ and $FeCl_3$ (black line) and of the MNps suspension (brown line). A well-defined band at 300 nm appears in the spectral of the mixture of Fe^{2+} and Fe^{3+}, attributed to the ligand-metal charge transfer (LMCT) transition in aqua-iron complexes in solution.[29] However, the spectrum of MNps had no defined bands, as also reported by Marangoni and co-authors[29] and Correa-Duarte and co-authors.[30] Furthermore, the baseline increased due to the scattering of light on the surface of MNps, a typical behavior of magnetic iron oxide on a nanoscale.[31,32] According to Mie's theory,[33] this increase is also attributable to the radiation absorbed (α_{abs}) by MNps and scattered radiation (α_{sca}), where extinction (α_{ext}) (or total extinction) is given by Equation 2.

$$\alpha_{ext} = \alpha_{sca} + \alpha_{abs} \quad (2)$$

Figure 3b shows a qualitative test with the application of an external field in the MNPs suspension. This applied field attracted MNps, suggesting that the nanoparticles have a magnetic behavior.

Another important parameter in understanding the optical properties of MNps is obtaining the band gap energy value. In this aspect, the method of extrapolating the tangent line of the Tauc graph (ahn *versus* energy) was used. As seen in Figure 3c, the energy value of the indirect band gap was 2.2 eV. This band gap energy value is in accordance with other works in the literature.[34-36]

3.2. Morphological characterization

The formation of the iron oxide on a nanoscale was confirmed by FEG-SEM images. Figures 4a to 4c show the polydisperse nanoparticles in the PDAC polymer matrix and a few aggregates. The PDAC polymer stabilized excessive growth, inhibiting the agglomeration of particles. In addition, MNps have a predominant spherical geometry and a relatively uniform particle size. According to FEG-SEM and other images, the average diameter of MNps is about 22 nm, as shown in the histogram of Figure 4d.

3.3. Photodegradation of tartrazine yellow dye

Photodegradation experiments were performed by adding 0.5 mg L^{-1} of MNps directly into the dye solution. The spectra were performed in the 350 to 550 nm region and recorded during the photodegradation time of 0 to 120 minutes. Initially, photodegradation was performed without MNps, as seen Figure 5a. This figure shows a broader band with λ_{max} at 420 nm when the time was 0 minutes. This band is attributed to the electronic transitions of the (-N=N-) azo group existing in the dye chemical structure (Figure 1).[37,38] At the beginning of the photodegradation of tartrazine yellow dye, the intensity of the absorption band slightly reduced after 15 minutes and remained practically constant until 120 minutes (Figure 5a). This decrease in the absorption band intensity with a wavelength of 420 nm can be attributed to the photolysis of the dye.

However, the spectroscopic behavior of dye photodegradation with MNps was different. Figure 5b shows that the increase in the time of photodegradation significantly decreased the maximum absorbance at all times. This augmentation in the dye removal efficiency is attributed to the presence of MNps. Figure 5c shows the graph of dye concentration as a function of photodegradation time.

The dye removal efficiency of the solution at 120 minutes was 30 and 96% without and with MNps, respectively. Comparison of the maximum percentage reduction of dye concentration using the MNp hybrids with other works reported in the literature was done. Generally, parameters such as initial dye concentration, contact time, reaction temperature, pH and the quantity of adsorbent are different in each work, making direct comparison difficult. However, when analyzing the percentage of removal as a function of the time in other works, it is noted that for percentages of 95 to 100% of dye removal generally occurs for times above 120 minutes of exposure to UV irradiation, as reported in Table 1. Thus, for this work, 96% dye degradation is reached in 120 minutes, demonstrating that the PDAC/Fe_3O_4 nanohybrid interface plays a fundamental role in the dye photocatalysis mechanism.

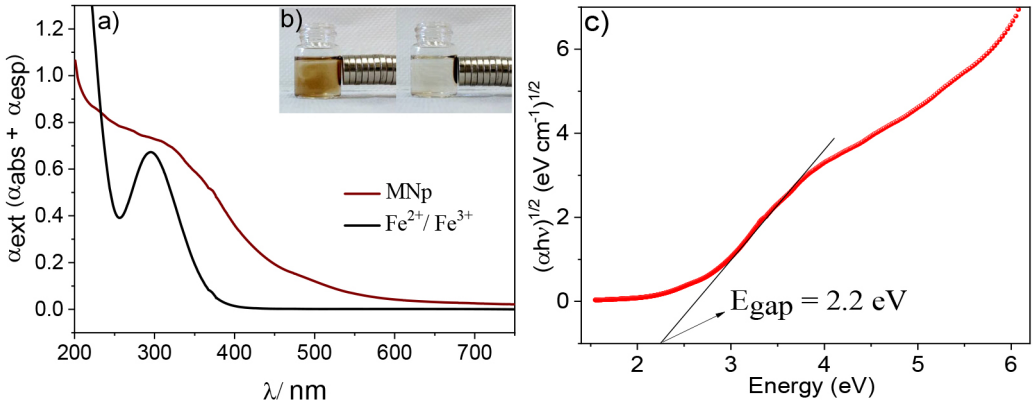

Figure 3. (a) UV-VIS spectra of the Fe^{2+}/Fe^{3+} solution (black line) and of the MNps suspension (brown line); (b) MNps suspension before and after application of an external magnetic field; (c) Tauc plot showing the indirect band gap energy value for MNps

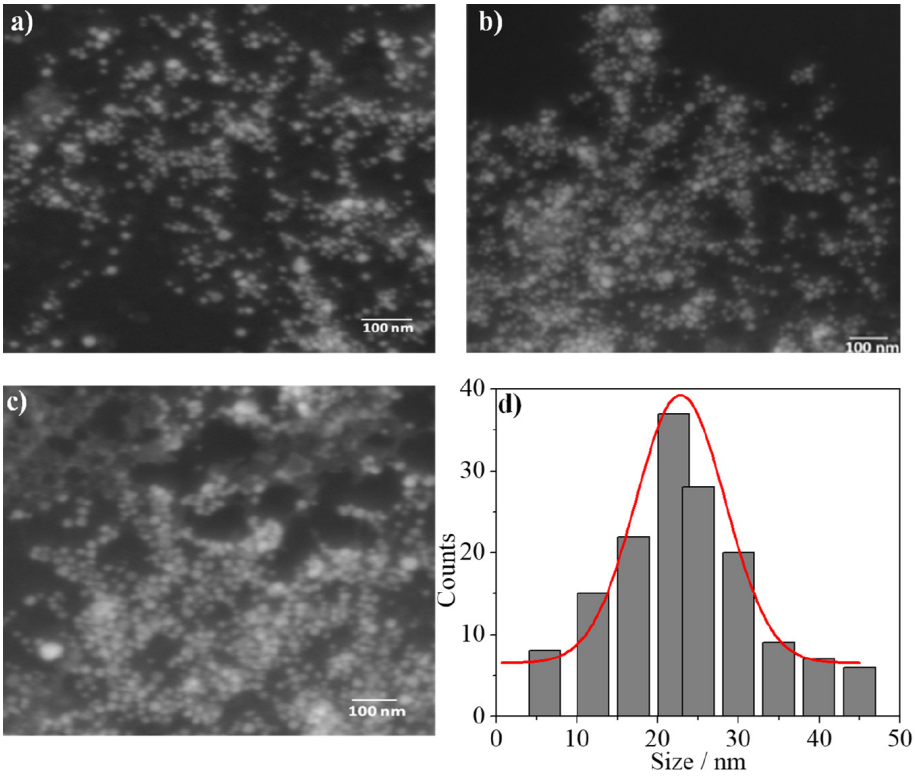

Figure 4. (a-c) FEG-SEM images of magnetic nanoparticles and (d) typical particle size histogram obtained from FEG-SEM data

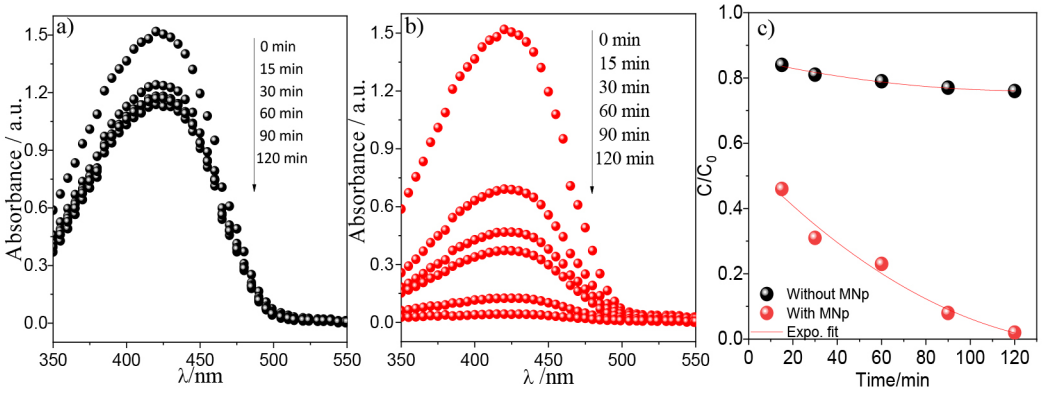

Figure 5. Absorbance curves at different exposure times of dye photodegradation (a) with and (b) without magnetic nanoparticles (c) graph of dye concentration as a function of photodegradation time

Table 1. Degradation percentage and exposure time values of literature works.

Nanoparticle system	Dye	Removal (%)	UV exposure time (min)	Ref.
Fe_3O_4@ZnS	Victoria blue R	93.94	120	39
Fe_3O_4/TiO_2	Rhodamine B	91	120	40
Fe_3O_4/AC/TiO_2	Methylene blue	84	120	41
Ru/Fe_3O_4	Methylene blue	90	120	42
PDAC/Fe_3O_4	Yellow tartrazine	96	120	This work

The greater dye removal efficiency in the presence of MNps may be attributed to two factors. First, iron oxide in MNps is a semiconductor material with nanometric dimensions. The average MNp diameter of 22 nm, seen in the FEG-SEM images, provides a greater number of e^-/h^+ pairs on the semiconductor surface, due to the large surface area of MNps.[8] This characteristic proportionally increases the radical species that react with the azo group of the dye.

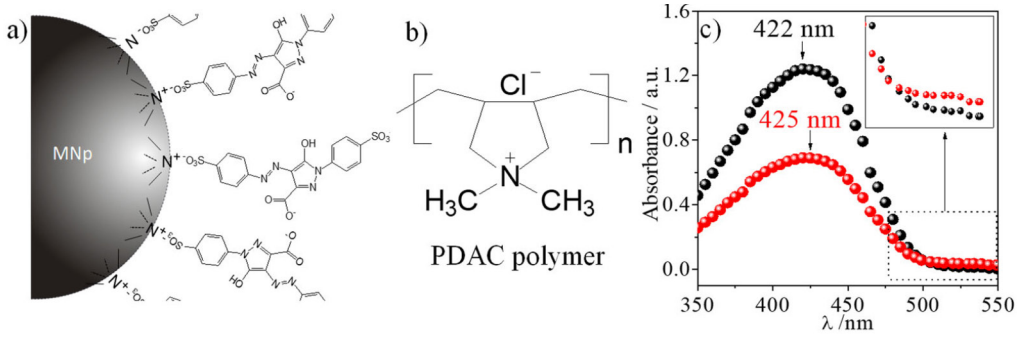

Figure 6. (a) Schematic representation proposal for the electrostatic interaction between magnetic nanoparticles (MNps) and tartrazine yellow dye; (b) Chemical structure of the PDAC polymer; (c) UV-VIS spectra at 15 min in the absence (black line) and presence (red line) of MNps. Inset shows the increase in the baseline of dye due the presence of MNps

Second, in the beginning of photodegradation, the dye was adsorbed on the nanohybrid surface by electrostatic interaction,[43,44] as seen in the proposed scheme in Figure 6a. In aqueous solution, the PDAC polymer coating MNps acquired a positive charge due to the presence of the quaternary amine (N^+) (Figure 6b). This positive site of MNps electrostatically interacted with the (O^-) present in the dye chemical structure. This interaction may be evidenced by overlaying the photodegradation spectra at 15 minutes of the reactions with and without MNps (Figure 6c). In Figure 6c, two behaviors can be observed: first, a bathochromic shift from 422 to 425 nm, and second, an increase in the baseline, as seen in inset in Figure 6b. The increase in the baseline occurs due to the scattering of light by the surface of MNps.

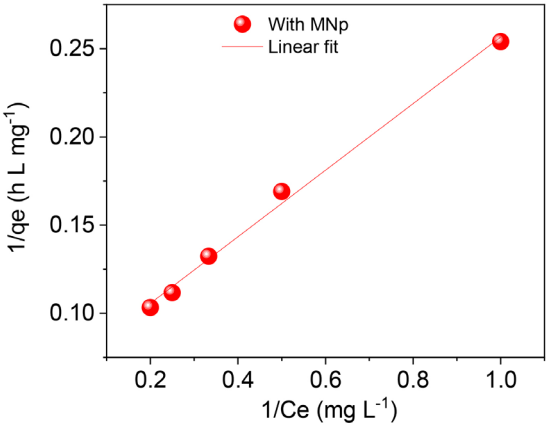

Figure 7. Linearized isotherm for dye photodegradation with of magnetic nanoparticles (MNp)

3.4. Kinetic study

Considering that photodegradation occurs at the solid-liquid interface, the rate of tartrazine degradation depends on its adsorption/photodegradation on the surface of MNps and the capacity of the MNps to generate e^-/h^+ pairs. Thus, to determine these parameters, the linearized Langmuir-Hinshelwood Equation 1 was used. When constructing the graph of the linearized isotherm for the reaction system between the PDAC-Fe_3O_4 nanohybrid and the tartrazine yellow dye, the graph in Figure 7 is obtained. As the experimental data present a linear regime according to the fit, this indicates that the adsorption/photodegradation capacity of the nanohybrid increases as the dye concentration increases. From the data extracted from this graph (angular and linear coefficient), the values for the constants $\mathbf{K_L}$ and $\mathbf{q_m}$ were obtained, respectively, as 14.72 and 0.36 mg L^{-1}.

The Langmuir R_L parameter is a dimensionless constant, known as the separation factor, which can be used to determine whether the dye adsorption/photodegradation process on the surface of adsorbents is favorable or not ($0 < R_L < 1$). This parameter is calculated by Equation 3.

$$R_L = \frac{1}{1 + K_L \times C_0} \quad (3)$$

The separation factor (R_L) ranged from 0.84 to 0.96, showing that the adsorption/photodegradation between tartrazine yellow dye and nanohybrid used are favorable processes, since the values are between 0 and 1. The kinetic parameters obtained for the PDAC-Fe_3O_4 system are in agreement with others reported in the literature such as described by Ayanda and co-authors[45] and Noruozi and co-authors[46] for similar magnetic systems, and indicates a strong adsorption reaction between the nanohybrid surface and the tartrazine yellow dye.

Based on these results, a photodegradation mechanism processed in two steps can be proposed: i) the electrostatic interaction between the surface of the MNp-PDAC nanohybrid and tartrazine yellow dye; ii) the generation of radicals on the surface of the MNp-PDAC nanohybrid. After the initial electrostatic interaction between MNps and the dye, the MNps were photoexcited by UV incidence. On the nanohybrid surface, the photoexcitation generates negative electrons (e^-_{CB}) in the conduction band and positive holes (h^+_{VB}) in the valence band. The photoinduced electron–hole pairs can either recombine or be captured by other molecules, such as water or oxygen, forming reactive oxygen species (ROS) such as hydroxyl radical ($OH^•$) and superoxide radical anion ($•O_2^-$). These ROS attacks the azo group of tartrazine yellow dye, and may lead to the formation of non-toxic carbon dioxide and

water.[36] The scheme in Figure 8 illustrates the photoinduction of electron-hole pairs, the generation of ROS, and the attacks to the chemical structure of dye in aqueous medium.

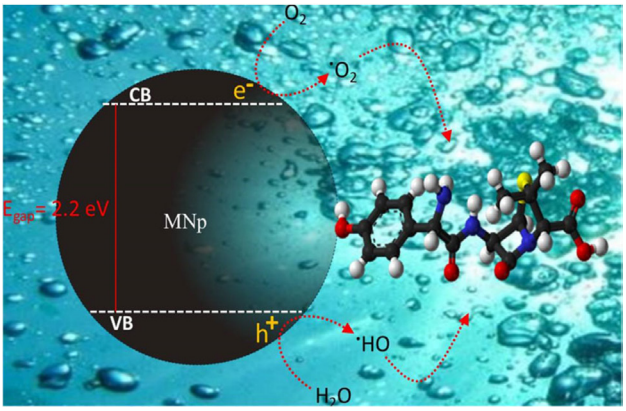

Figure 8. Schematic representation of the photoinduction of / pairs, the generation of ROS, and the attacks to the chemical structure of dye in aqueous medium

4. Conclusions

This work showed the photodegradation of tartrazine yellow dye with and without MNp-PDAC nanohybrid. In the presence of the nanohybrid, the dye removal efficiency was 96%, as opposed to the removal efficiency of 30% in the absence of nanohybrid. The fast photodegradation kinetics and the high percentage value of dye removal can be attributed to the electrostatic attraction between the PDAC polymer coating MNps and tartrazine yellow dye. Thus, this material is promising for the decontamination of wastewater with anionic organic dyes in order to be magnetically reusable.

Acknowledgements

The authors gratefully thank PIBIC-EM/IFG, PPG-Química/UFCAT, CAPES, and financial support from IFGOIANO/PROPPI, Resolution nº 064/2014 for translating and processing the article.

References

1. Lanjwani, M. F.; Tuzen, M.; Khuhawar, M. Y.; Saleh, T. A.; Trends in photocatalytic degradation of organic dye pollutants using nanoparticles: A review. *Inorganic Chemistry Communications* **2024**, *159*, 111613. [Crossref]
2. Abd Elkodous, M.; El-Khawaga, A. M.; Abouelela, M. M.; Abdel Maksoud, M. I. A.; Cocatalyst loaded Al-$SrTiO_3$ cubes for Congo red dye photo-degradation under wide range of light. *Scientifc Reports* **2023**, *13*, 6331. [Crossref]
3. Asghar, H.; Khan, I.; Saeed, M.; Wu, P.; Khan, A.; Synthesis of g-C_3N_4/$SmFeO_3$ nanosheets Z-scheme based nanocomposites as efficient visible light photocatalysts for CO_2 reduction and Congo red degradation. *Journal of Materials Research* **2023**, *38*, 2986. [Crossref]
4. Al-Kadhi, N. S.; Saad, F. A.; Shah, R. K.; El-Sayyad, G. S.; Alqahtani, Z.; Abdelrahman, E. A.; Photocatalytic Decomposition of Indigo Carmine and Methylene Blue Dyes Using Facilely Synthesized Lithium Borate/Copper Oxide Nanocomposite. *Journal of Inorganic and Organometallic Polymers and Materials* **2023**, *33*, 2765. [Crossref]
5. Menezes, L. B.; Muraro, P. C. L.; Druzian, D. M.; Ruiz, Y. P. M.; Galembeck, A.; Pavoski, G.; Espinosa, D. C. R.; Silva, W. L.; Calcium oxide nanoparticles: Biosynthesis, characterization and photocatalytic activity for application in yellow tartrazine dye removal. *Journal of Photochemistry and Photobiology A: Chemistry* **2024**, *447*, 115182. [Crossref]
6. Sudhaik, A.; Raizada, P.; Shandilya, P.; Jeong, D.-Y.; Lim, J.-H.; Singh, P.; Review on fabrication of graphitic carbon nitride based efficient nanocomposites for photodegradation of aqueous phase organic pollutants. *Journal of Industrial and Engineering Chemistry* **2018**, *67*, 28. [Crossref]
7. Mahmoodi, N. M.; Arami, M.; Limaee, N. Y.; Tabrizi, N. S.; Kinetics of heterogeneous photocatalytic degradation of reactive dyes in an immobilized TiO_2 photocatalytic reactor. *Journal of Colloid and Interface Science* **2006**, *295*, 159. [Crossref]
8. Liu, Y.; Yu, L.; Hu, Y.; Guo, C.; Zhang, F.; Lou, X. W. D.; A magnetically separable photocatalyst based on nest-like γ-Fe_2O_3/ZnO double-shelled hollow structures with enhanced photocatalytic activity. *Nanoscale* **2012**, *4*, 183. [Crossref]
9. Konstantinou, I. K.; Albanis, T. A.; TiO_2-assisted photocatalytic degradation of azo dyes in aqueous solution: kinetic and mechanistic investigations: A review. *Applied Catalysis B: Environmental* **2004**, *49*, 1. [Crossref]
10. Zhang, Z. Y.; Shao, C. L.; Li, X. H.; Zhang, L.; Xue, H. M.; Wang, C. H.; Liu, Y. C.; Electrospun Nanofibers of ZnO–SnO_2 Heterojunction with High Photocatalytic Activity. *Journal of Physical Chemistry C* **2010**, *114*, 7920. [Crossref]
11. Yang, L.-Y.; Dong, S.-Y.; Sun, J.-H.; Feng, J.-L.; Wu, Q.-H.; Sun, S.-P.; Microwave-assisted preparation, characterization and photocatalytic properties of a dumbbell-shaped ZnO photocatalyst. *Journal of Hazardous Materials* **2010**, *179*, 438. [Crossref]
12. Behnajady, M. A.; Modirshahla, N.; Hamzavi, R.; Kinetic study on photocatalytic degradation of C.I. Acid Yellow 23 by ZnO photocatalyst. *Journal of Hazardous Materials* **2006**, *133*, 226. [Crossref]
13. Daneshvar, N.; Salari, D.; Khataee, A. R.; Photocatalytic degradation of azo dye acid red 14 in water on ZnO as an alternative catalyst to TiO_2. *Journal of Photochemistry and Photobiology A: Chemistry* **2004**, *162*, 317. [Crossref]
14. Kiani, A.; Nabiyouni, G.; Masoumi, S.; Ghanbari, D.; A novel magnetic $MgFe_2O_4$–$MgTiO_3$ perovskite nanocomposite: Rapid photo-degradation of toxic dyes under visible irradiation. *Composites Part B: Engineering* **2019**, *175*, 107080. [Crossref]
15. Mengting, Z.; Kurniawan, T. A.; Yanping, Y.; Othman, M. H. D.; Fu, R. A. D.; Hwang, G. H.; Fabrication, characterization, and application of ternary magnetic recyclable Bi_2WO_6/BiOI@Fe_3O_4

composite for photodegradation of tetracycline in aqueous solutions. *Journal of Environmental Management* **2020**, *270*, 110839. [Crossref]

16. Sanad, M. M. S.; Farahat, M. M.; El-Hout, S. I.; El-Sheikh, S. M.; Preparation and characterization of magnetic photocatalyst from the banded iron formation for effective photodegradation of methylene blue under UV and visible illumination. *Journal of Environmental Chemical Engineering* **2021**, *9*, 105127. [Crossref]
17. Ullah, R.; Dutta, J.; Photocatalytic degradation of organic dyes with manganese-doped ZnO nanoparticles. *Journal of Hazardous Materials* **2008**, *156*, 194. [Crossref]
18. Curri, M. L.; Comparelli, R.; Cozzoli, P. D.; Mascolo, G.; Agostiano, A.; Colloidal oxide nanoparticles for the photocatalytic degradation of organic dye. *Materials Science and Engineering: C* **2003**, *23*, 285. [Crossref]
19. Pouretedal, H. R.; Norozi, A.; Keshavarz, M. H.; Semnani, A.; Nanoparticles of zinc sulfide doped with manganese, nickel and copper as nanophotocatalyst in the degradation of organic dyes. *Journal of Hazardous Materials* **2009**, *162*, 674. [Crossref]
20. Rana, S.; Srivastava, R. S.; Sorensson, M. M.; Misra, R. D. K.; Synthesis and characterization of nanoparticles with magnetic core and photocatalytic shell: Anatase TiO_2–$NiFe_2O_4$ system. *Materials Science and Engineering: B* **2005**, *119*, 144. [Crossref]
21. Guo, J. F.; Ma, B.; Yin, A.; Fan, K.; Dai, W. L.; Photodegradation of rhodamine B and 4-chlorophenol using plasmonic photocatalyst of Ag–AgI/Fe_3O_4@SiO_2 magnetic nanoparticle under visible light irradiation. *Applied Catalysis B: Environmental* **2011**, *101*, 580. [Crossref]
22. Długosz, O.; Szostak, K.; Krupiński, M.; Banach, M.; Synthesis of Fe_3O_4/ZnO nanoparticles and their application for the photodegradation of anionic and cationic dyes. *International Journal of Environmental Science and Technology* **2021**, *18*, 561. [Crossref]
23. Fardood, S. T.; Moradnia, F.; Ramazani, A.; Green synthesis and characterisation of $ZnMn_2O_4$ nanoparticles for photocatalytic degradation of Congo red dye and kinetic study. *Micro & Nano Letters* **2019**, *14*, 986. [Crossref]
24. Lonski, S.; Lukowiec, D.; Barbusinski, K.; Babilas, R.; Szeląg, B.; Radon, A.; Flower-like Magnetite Nanoparticles with Unfunctionalized Surface as an Efficient Catalyst in Photo-Fenton Degradation of Chemical Dyes. *Applied Surface Science* **2023**, *638*, 158127. [Crossref]
25. Jadhav, A.; Chavan, R.; Sonawane, S.; Kamble, P.; Mahajan, S.; Vhankhande, B.; Ghorpade, R.; Chougale, A.; Abd El-Salam, N. M.; Fouad, H.; Patil, R.; Photocatalytic Degradation of Crystal Violet Dye Using Iron Oxide Nanoparticles. *Journal of Nanoeletronics and Optoeletronics* **2024**, *19*, 272. [Crossref]
26. Martins, M. V. A.; Bonfim, C.; Silva, W. C.; Crespilho, F. N.; Iron (III) nanocomposites for enzyme-less biomimetic cathode: A promising material for use in biofuel cells. *Electrochemistry Communication* **2010**, *12*, 1509. [Crossref]
27. Laurent, S.; Forge, D.; Port, M.; Roch, A.; Robic, C.; Elst, L. V.; Muller, R. N.; Magnetic Iron Oxide Nanoparticles: Synthesis, Stabilization, Vectorization, Physicochemical Characterizations, and Biological Applications. *Chemical Review* **2008**, *108*, 2064. [Crossref]
28. Melo, A. F. A. A.; Luz, R. A. S.; Iost, R. M.; Nantes, I. L.; Crespilho, F. N.; Highly Stable Magnetite Modified with Chitosan, Ferrocene and Enzyme for Application in Magneto-Switchable Bioelectrocatalysis. *Journal of the Brazilian Chemical Society* **2013**, *24*, 285. [Crossref]
29. Marangoni, V. S.; Martins, M. V. A.; Souza, J. A.; Oliveira, O. N.; Zucolotto, V.; Crespilho, F. N.; The processing of polyelectrolyte-covered magnetite nanoparticles in the form of nanostructured thin films. *Journal of the Nanoparticle Research* **2012**, *14*, 769. [Crossref]
30. Correa-Duarte, M. A.; Giersig, M.; Kotov, N. A.; Liz-Marzan, L. M.; Control of Packing Order of Self-Assembled Monolayers of Magnetite Nanoparticles with and without SiO_2 Coating by Microwave Irradiation. *Langmuir* **1998,** *14*, 6430. [Crossref]
31. Kaushik, A.; Khan, R.; Solanki, P. R.; Pandey, P.; Alam, J.; Ahmad, S.; Malhotra, B. D.; Iron oxide nanoparticles–chitosan composite based glucose biosensor. *Biosensors and Bioelectronics* **2008**, *24*, 676. [Crossref]
32. Zhang, X. Q.; Gong, S. W.; Zhang, Y.; Yang, T.; Wang, C. Y.; Gu, N.; Prussian blue modified iron oxide magnetic nanoparticles and their high peroxidase-like activity. *Journal of Materials Chemistry* **2010**, *20*, 5110. [Crossref]
33. 33. Tang, Y.-L.; Yen, T.-H.; Nishida, K.; Li, C.-H.; Chen, Y.-C.; Zhang, T.;Pai, C.-K.; Chen, K.-P.; Li, X.; Takahara, J.; Chu, S.-W.; Multipole engineering by displacement resonance: a new degree of freedom of Mie resonance. *Nature Communication* **2023**, *14*, 7213. [Crossref]
34. Donya, H.; Taha, T. A.; Alruwaili, A.; Tomsah, I. B. I.; Ibrahim, M.; Micro-structure and optical spectroscopy of PVA/iron oxide polymer nanocomposites. *Journal of Materials Research and Technology* **2020**, *9*, 9189. [Crossref]
35. Sri V, S. P. S.; Taj, J.; George, M.; Facile synthesis of magnetite nanocubes using deep eutectic solvent: an insight to anticancer and photo-Fenton efficacy. *Surfaces and Interfaces* **2020**, *20*, 100609. [Crossref]
36. Raha, S.; Ahmaruzzaman, M.; Facile fabrication of g-C_3N_4 supported Fe_3O_4 nanoparticles/ZnO nanorods: A superlative visible light responsive architecture for express degradation of pantoprazole. *Chemical Engineering Journal* **2020**, *387*, 123766. [Crossref]
37. Stylidi, M.; Kondarides, D. I.; Verykios, X. E.; Visible light-induced photocatalytic degradation of Acid Orange 7 in aqueous TiO_2 suspensions. *Applied Catalysis B: Environmental* **2004**, *47*, 189. [Crossref]
38. Oancea, P.; Meltzer, V.; Photo-Fenton process for the degradation of Tartrazine (E102) in aqueous medium. *Journal of the Taiwan Institute of Chemical Engineers* **2013**, *44*, 990. [Crossref]
39. Karimi, H.; Rajabi, H. R.; Kavoshi, L.; Application of decorated magnetic nanophotocatalysts for efficient photodegradation of organic dye: A comparison study on photocatalytic activity of magnetic zinc sulfide and graphene quantum dots. *Journal of Photochemistry and Photobiology A: Chemistry* **2020**, *397*, 112534. [Crossref]
40. Madima, N.; Kefeni, K. K.; Mishra, S. B.; Mishra, A. K.; Kuvarega, A. T.; Fabrication of magnetic recoverable Fe_3O_4/TiO_2 heterostructure for photocatalytic degradation of rhodamine B

dye. *Inorganic Chemistry Communications* **2022**, *145*, 109966. [Crossref]

41. Moosavi, S.; Li, R. Y. M.; Lai, C. W.; Yusof, Y.; Gan, S.; Akbarzadeh, O.; Johan, M. R.; Chowhury, Z. Z.; Yue, X. G.; Methylene blue dye photocatalytic degradation over synthesised Fe_3O_4/AC/TiO_2 nano-catalyst: degradation and reusability studies. *Nanomaterials* **2020**, *10*, 2360. [Crossref]
42. Kumar, A. P.; Ahmed, F.; Kumar, S.; Anuradha, G.; Harish, K.; Kumar, B. P.; Lee, Y. I.; Synthesis of Magnetically Recoverable Ru/Fe_3O_4 Nanocomposite for Efficient Photocatalytic Degradation of Methylene Blue. *Journal of Cluster Science* **2022**, *33*, 853. [Crossref]
43. Reddy, D. H. K.; Lee, S.-M.; Application of magnetic chitosan composites for the removal of toxic metal and dyes from aqueous solutions. *Advances in Colloid and Interface Science* **2013**, 68, *201*. [Crossref]
44. Chang, Y.-C.; Chen, D.-H.; Adsorption Kinetics and Thermodynamics of Acid Dyes on a Carboxymethylated Chitosan-Conjugated Magnetic Nano-Adsorbent. *Macromolecular Bioscience* **2005**, *5*, 254. [Crossref]
45. Ayanda, O. S.; Oforkansi, C. C.; Aremu, O. H.; Ogunjemiluyi, O. E.; Olowoyeye, O. L.; Akintayo, C. O.; Degradation of Amido Black Dye Using Ultra-Violet Light Catalyzed by Iron Oxide Nanoparticles: Kinetics and Mechanism of Degradation. Catalysis Research 2022, *2*, 22. [Crossref]
46. Noruozi, A.; Nezamzadeh-Ejhieh, A.; Preparation, characterization, and investigation of the catalytic property of α-Fe_2O_3-ZnO nanoparticles in the photodegradation and mineralization of methylene blue. *Chemical Physics Letters* **2020**, 752, 137. [Crossref]